Developing a coral proxy system model to compare coral and climate model estimates of changes in paleo-ENSO variability

A.E. Lawman[1,2]*, J.W. Partin[1], S.G. Dee[3], C.A. Casadio[1], P. Di Nezio[1], T.M. Quinn[1,2]

[1]Institute for Geophysics, Jackson School of Geosciences, The University of Texas at Austin, Austin, TX, USA. [2]Department of Geological Sciences, Jackson School of Geosciences, The University of Texas at Austin, Austin, TX, USA. [3]Department of Earth, Environmental and Planetary Sciences, Rice University, Houston, TX, USA.

Corresponding author: Allison Lawman (alawman@utexas.edu)

This is a non peer-reviewed preprint submitted to EarthArXiv. The article was submitted to *Paleoceanography and Paleoclimatology* on December 16, 2019.

Key Points:

- We present a new coral proxy system model to facilitate comparison between proxy observations and climate model output
- Analytical and calibration errors, variable growth rates, and age modeling uncertainties all have measurable impacts on interannual variance
- The relative importance of different uncertainties on interannual variance are site-dependent

Abstract

Coral records of surface-ocean conditions extend our knowledge of interannual El Niño-Southern Oscillation (ENSO) variability into the pre-instrumental period. That said, internal variability within the climate system as well as multiple sources of uncertainties inherent to the coral archive produce challenges for the paleoclimate community to detect forced changes in ENSO using coral geochemical records. We present a new coral proxy system model (PSM) of intermediate complexity, geared toward the evaluation of changes in interannual variance. Our coral PSM adds additional layers of complexity to previously published transfer functions that describe how the archive responds to sea-surface temperature (SST) and salinity. We use SST and salinity output from the Community Earth System Model Last Millennium Ensemble 850 control to forward-model coral oxygen isotopic ratios and SST derived from Sr/Ca. We present a detailed analysis of our coral PSM using climate model output for sites in the central and southwest Pacific before subsequently extending the analyses to span the broader tropical Pacific. We demonstrate how analytical and calibration errors, variable growth rates, and age model assumptions systematically change interannual variance, and show that the relative magnitude of the variance change is location dependent. Importantly, however, we find that even with the added uncertainties in our PSM, corals spanning the circum-Pacific are broadly able to capture decadal and longer (decadal+) changes in ENSO variability. Our code is publicly available to the broader community and documented on GitHub to facilitate future comparisons between model output and coral proxy data.

Plain Language Summary

Climate scientists use the chemistry of coral skeletons to study past tropical climate conditions. Specifically, the elemental ratio of strontium to calcium (Sr/Ca) and the oxygen isotopic composition ($\delta^{18}O$) in the coral skeleton have demonstrated utility. Coral Sr/Ca varies in response to changes in sea-surface temperature, whereas coral $\delta^{18}O$ records both changes in temperature and salinity. Individual corals provide tens to hundreds of years of climate information from the tropical oceans. They are well-suited for studying variability related to the El Niño-Southern Oscillation (ENSO), a climate phenomenon that impacts global temperature and rainfall patterns every few years. We rely on both climate proxy data and simulations from global climate models to study changes in ENSO variability in the past. Nevertheless, it is difficult to directly compare proxy data with climate model output due to the imperfect nature of how the climate signal is recorded in the coral skeleton. Proxy system models are a tool designed to help bridge the gap between climate information recorded in corals and climate model output. In this study, we develop a coral proxy system model to demonstrate how different processes impact a coral's ability to record changes in ENSO variability.

1 Introduction

Geochemical records from massive corals provide decades to centuries of sub-annually resolved proxy climate data from the tropical oceans [*Fairbanks et al.*, 1997; *Gagan et al.*, 2000; *Lough*, 2010]. The ratio of strontium to calcium (Sr/Ca) and the oxygen isotopic composition ($\delta^{18}O$) of coral skeletal material are established climate proxies [*Fairbanks et al.*, 1997; *Corrège*, 2006; *Lough*, 2010; *DeLong et al.*, 2013]. Sea-surface temperature (SST) exerts the dominant climate control on coral Sr/Ca [*Weber*, 1973; *Smith et al.*, 1979; *Beck et al.*, 1992], whereas coral $\delta^{18}O$ is jointly influenced by SST and the oxygen isotopic composition of seawater ($\delta^{18}O_{sw}$) [*Weber and Woodhead*, 1972; *Gagan et al.*, 1998; *Ren et al.*, 2003], the latter of which is impacted by similar processes as sea-surface salinity (e.g., rainfall, evaporation, advection of different water masses, and freshwater runoff) [*LeGrande and Schmidt*, 2006]. Geochemical records from tropical Pacific corals provide insight into El Niño-

Southern Oscillation (ENSO) variability, the leading mode of interannual climate variability with global impacts on temperature and precipitation patterns [*Bjerknes*, 1969; *Ropelewski and Halpert*, 1987].

SST anomalies (SSTA) averaged across the Niño 3.4 region in the central equatorial Pacific (5°N-5°S, 120-170°W), shows an increase in the magnitude and frequency of extreme ENSO events over the last few decades [*Trenberth and Hoar*, 1996; *Bin Wang et al.*, 2019]. However, instrumental observations are of insufficient length [*Fairbanks et al.*, 1997; *Deser et al.*, 2010] to characterize the full range of internal variability [*Wittenberg*, 2009]. Model simulations of future ENSO changes differ widely in response to both external forcing of increasing greenhouse gas emissions and internal variability in the climate system [*Collins et al.*, 2010; *DiNezio et al.*, 2013; *Bellenger et al.*, 2014; *Cai et al.*, 2014; 2015]. Coral-based climate records that overlap with, and extend beyond, the instrumental period provide tests of climate model simulations of ENSO [*Gagan et al.*, 2000; *Cobb et al.*, 2013; *Schmidt et al.*, 2014].

There are, however, several sources of uncertainty that impact our ability to understand past changes in ENSO variability, including those due to the climate system and from the coral archive. ENSO behavior can vary in the absence of forcings external to the climate system [*Wittenberg*, 2009; *Deser et al.*, 2012], making it difficult to separate internally versus externally driven changes in variability from short (several decades or less) coral records. There also needs to be a clear link between variability at the individual reef site and ENSO. Lastly, the coral archive itself impacts how a climate signal is recorded. These sources of uncertainty are summarized as follows:

1. The ability of a point-source location to capture regional changes in ENSO variability
2. Internal variability of the climate system
3. The ability of coral Sr/Ca and $\delta^{18}O$ to record ocean-climate variables
4. Uncertainties in the coral archive that may obfuscate the climate signal of interest (e.g., variable growth rates)
5. Proxy observation uncertainties (e.g., analytical, calibration, dating, and age-model errors)

A proxy system model (PSM) addresses some of these challenges and serves as an important bridge between proxy data and observations or model output [*Evans et al.*, 2013; *Dee et al.*, 2015], as one can mathematically model how different processes impact a climate signal that emerges from the proxy data. Typically, paleoclimate proxy data is transformed back into a climate variable (e.g., SST) using empirically determined calibration equations [*Corrège*, 2006]. Conversely, forward modeling via a PSM transforms observations or climate model output into "pseudoproxies" that estimate the proxy signal [*Evans et al.*, 2013; *Dee et al.*, 2015].

In this study, we use surface temperature and salinity output from the Community Earth System Model Last Millennium Ensemble (CESM-LME) to forward model "pseudocoral" [*Brown et al.*, 2008] $\delta^{18}O$ and SST derived from Sr/Ca ($SST_{Sr/Ca}$). We first focus on the central (Christmas Island) and southwest Pacific (Vanuatu) to demonstrate the subcomponents of our PSM, and then expand our pseudoproxy network to span the tropical Pacific. Our coral PSM adds layers of complexity to the transfer functions that describe how the archive responds to SST and salinity [*Thompson et al.*, 2011; *Dee et al.*, 2015]. We identify how uncertainties associated with 1) analytical and calibration errors, 2) variable growth rates, and 3) age modeling assumptions, impact interannual variance and the ability of a pseudocoral to capture decadal and longer (decadal+) changes in ENSO variability. Although precise month-to-month SST variations in the Niño 3.4 region are a common target for ENSO studies, this is challenging for paleoclimate studies because of temporal uncertainties in proxy records [*Emile-*

Geay et al., 2013a; 2013b]. Thus, we focus on how various coral processes impact estimates of decadal+ changes in ENSO variability in coral paleoclimate reconstructions. Sections 2 and 3 describe the coral PSM framework. Coral archive uncertainties on interannual variance as well as a coral's ability to capture changes in ENSO variability are presented in section 4. Conclusions are provided in section 5.

2 Coral PSM Framework

Proxy system models are tools used to evaluate the contribution of local environmental signals and their variability on the measured proxy record. Coral PSMs have previously been used to make more advanced comparisons between observations and climate model data [*Thompson et al.*, 2011], quantify uncertainties in signal interpretation [*Dee et al.*, 2015], and quantify errors in coral-based ENSO amplitude [*Russon et al.*, 2015] or variability estimates [*Stevenson et al.*, 2013]. Here, we introduce a coral PSM that builds upon previous work and adds new layers of complexity by incorporating uncertainties related to:

1. Variable growth rates experienced when sampling a coral along the maximum growth axis
2. Analytical and calibration errors
3. Seasonal chronological uncertainties associated with transforming coral geochemical data from the depth to the time domain (herein referred to as the age model)

Our design adheres to the PSM framework described in *Evans et al.* [2013] where a PSM consists of environment, sensor, archive, and observation subcomponents (Figure 1). This is the first study that includes an archive-based coral PSM with a variable growth rate algorithm. Analytical and calibration errors as well as the age model assumptions fall within the observation PSM. Our coral PSM is optimized to use Monte Carlo methods to run any permutation of the various archive and observation sub-models (Figure 1 arrows) and generate *n* realizations of pseudocoral $\delta^{18}O$ or $SST_{Sr/Ca}$. This study focuses on how various uncertainties impact interannual variance, a leading timescale of interest for coral-based paleoclimatology.

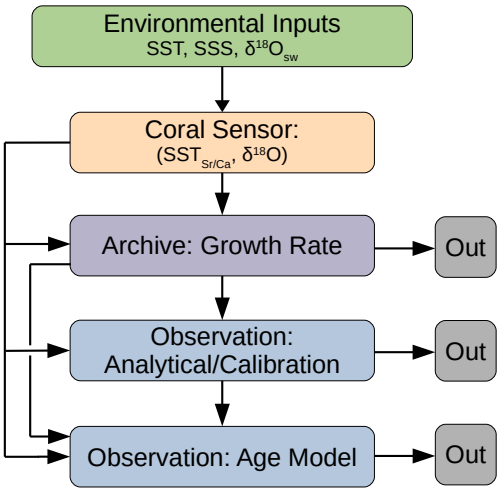

Figure 1. Coral proxy system model (PSM) schematic. The sea-surface temperature (SST), sea-surface salinity (SSS), or the oxygen isotopic composition of sea water ($\delta^{18}O_{sw}$) environmental inputs (green box) can come from instrumental observations, climate model output, or reanalysis data [*Evans et al.*, 2013; *Dee et al.*, 2015]. Here and in all subsequent figures, $SST_{Sr/Ca}$ refers to SST derived from coral Sr/Ca. The coral $\delta^{18}O$ sensor model [*Thompson et al.*, 2011] accounts for sensitivity to SST and $\delta^{18}O_{sw}$ (SSS). The growth rate archive model (purple box) describes how an environmental signal may be emplaced or transformed in the coral archive due to variable growth rates. The coral observation models (blue boxes) include the combined effect of analytical and calibration errors, as well as age model uncertainties that arise from transforming the coral geochemical from the depth to the time domain. Arrows shows possible permutations of the archive and observation sub-models to yield pseudocoral output. The full coral PSM refers to consecutively perturbing the environmental inputs with the growth rate, analytical/calibration, and age-model algorithms.

2.1 Coral PSM Input Variables

The environmental inputs for the coral PSM are SST, sea-surface salinity (SSS), and $\delta^{18}O_{sw}$ if available (Figure 1). These climate variables can be from instrumental observations or model output. Here we use surface temperature and salinity output from the CESM-LME 850 control as the

environmental inputs [*Otto-Bliesner et al.*, 2016]. The CESM-LME uses version 1.1 of CESM with the Community Atmospheric Model Version 5, CESM1(CAM5) [*Hurrell et al.*, 2013]. The CESM-LME uses ~2° resolution for the atmosphere and ~1° resolution for the ocean. Surface salinity data (0-10 m depth) was gridded to the same ~2° resolution as the atmospheric components to facilitate forward modeling coral $\delta^{18}O$ as a linear combination of SST and SSS. There are no changes in external forcing throughout the 850 control simulation [*Otto-Bliesner et al.*, 2016], hence all variability is internal. The long control allows us to sample across a wide range of internal variability, which is not possible in the short instrumental record, and to quantify how different assumptions and uncertainties inherent to the coral archive impact interannual variance in a geochemical time series.

Herein we seek to understand how different coral uncertainties impact interannual variance within the CESM-LME depiction of climate. We thus evaluate the proxy uncertainties within the simulated climate generated by the model, such that we constrain ourselves to the CESM-LME's simulation of tropical Pacific variability, including ENSO. The spatial patterns observed using the CESM-LME may not be strictly comparable to other models, but the general results about how the three coral uncertainties impact interannual variability are broadly applicable to environmental inputs from observations or other climate models. Due to model biases, we caution users of the PSM to avoid direct point-to-point comparisons between coral observations and climate model output from a single grid point. Care must be taken to select a broader region that best matches the climate conditions observed at the proxy site.

2.2. Coral Sensor Models

2.2.1 Pseudocoral $\delta^{18}O$

We use the sensor model of *Thompson et al.* [2011] to forward model mean-removed pseudocoral $\delta^{18}O$ anomalies ($\Delta\delta^{18}O_{pseudocoral}$) as a linear combination of SST and $\delta^{18}O_{sw}$ or salinity anomalies:

$$\Delta\delta^{18}O_{pseudocoral} = a_1\Delta SST + \Delta\delta^{18}O_{sw} \text{ (Eq. 1)}$$

$$\Delta\delta^{18}O_{pseudocoral} = a_1\Delta SST + a_2\Delta SSS \text{ (Eq. 2)}$$

The coefficient a_1 is based on the inverse SST dependence that arises from thermodynamic fractionation [*Epstein et al.*, 1953]. We use a slope -0.22 ‰/°C for a_1 as used in *Thompson et al.* [2011], but recognize that other slope values exist in the literature [*Evans et al.*, 2000].

SSS and $\delta^{18}O_{sw}$ are often assumed to be linearly proportional as they are impacted by similar precipitation, evaporation, and advection processes [*LeGrande and Schmidt*, 2006]. We use Eq. 2 and approximate a_2 using observed $\delta^{18}O_{sw}$-SSS slopes determined from basin-scale regression analysis [*LeGrande and Schmidt*, 2006]. Limited $\delta^{18}O_{sw}$ and SSS observations [*LeGrande and Schmidt*, 2006], spatiotemporal variability in the $\delta^{18}O_{sw}$-SSS relationship [*Conroy et al.*, 2017], or sub-grid processes affecting $\delta^{18}O_{sw}$ [*Stevenson et al.*, 2015] can lead to large errors on interannual variance [*Stevenson et al.*, 2013; *Russon et al.*, 2015] and hinder direct comparison between forward modeled pseudocorals and coral proxy observations. Since our study focuses on the impact of other processes on interannual variance we define a_2 as 0.27 for the tropical Pacific and 0.45 for the South Pacific as in *Legrande & Schmidt* [2006].

2.2.2 Pseudocoral SST Derived from Sr/Ca ($SST_{Sr/Ca}$)

The inverse relationship between coral Sr/Ca and temperature is an established proxy for reconstructing SST variability [*Beck et al.*, 1992; *Gagan et al.*, 2000; *Quinn and Sampson*, 2002;

190 *Corrège*, 2006; *Lough*, 2010]. Slope values for Sr/Ca-SST typically fall within the -0.06 ± 0.01 (±1σ)
191 mmol/mol/°C range for the Indo-Pacific [*Corrège*, 2006]. Uncertainties in the Sr/Ca-SST calibration
192 can yield errors in the SST reconstruction up to 0.35°C (±2σ) [*Quinn and Sampson*, 2002], although
193 this uncertainty may be higher based on interlaboratory comparisons [*Hathorne et al.*, 2013] and
194 reproducibility studies [*Sayani et al.*, 2019]. In this study we assume that the original SST input to
195 the coral PSM is a reasonable approximation of SST derived from coral Sr/Ca ($SST_{Sr/Ca}$). A published
196 coral Sr/Ca sensor model does not exist at the time of this study but could be incorporated into our
197 coral PSM framework in the future.
198
199 **2.3 Pseudocoral Case Studies: Christmas Island & Vanuatu**

200 ENSO involves basin-scale atmospheric and oceanic interactions across the tropical Pacific, with the
201 largest interannual signal occurring in the central and eastern equatorial Pacific. In contrast, coral
202 heads are from point-source locations (on the scale of meters) that are impacted by both regional and
203 local climate processes. Thus, there needs to be a demonstrated link between climate variability at the
204 individual reef site and ENSO. Modern and paleo-ENSO studies have targeted sites within the Niño
205 3.4 region [*Cobb et al.*, 2013; *Emile-Geay et al.*, 2016], as well as sites in the eastern, western, and
206 southwest Pacific that are sensitive to changes in ENSO variability [*Hereid et al.*, 2013a]. For
207 example, the western and southwest Pacific contain a large number of islands that are home to
208 abundant modern and fossil coral heads for paleoclimate studies [*Cole et al.*, 1993; *Kilbourne et al.*,
209 2004; *Linsley et al.*, 2006; *DeLong et al.*, 2012; *Gorman et al.*, 2012; *Hereid et al.*, 2013b; *Jimenez*
210 *et al.*, 2018; and many others].
211
212 We choose two end-member localities (Christmas (Kirimati) Island (2°N, 157°W); Vanuatu (16°S,
213 167°E) to apply our coral PSM for testing how different processes and uncertainties inherent to coral-
214 based paleoclimatology impact interannual variance. Christmas Island, located in the central
215 equatorial Pacific, has a small annual cycle and a large interannual response, whereas Vanuatu,
216 located within the SPCZ, has a larger annual cycle and a smaller interannual response. In all instances,
217 when selecting the SST or forward modeled $\Delta\delta^{18}O_{pseudocoral}$ (Eq. 2) input for the coral PSM, we use
218 the model output from the grid point closest to the selected sites.
219
220 **3. New PSM Design Following Laboratory and Analytical Practices for Coral Measurements**

221 The full coral PSM refers to consecutively perturbing the original environmental inputs with variable
222 growth rates, analytical and calibration errors, and the age modeling algorithm (Figure 1). The
223 following subsections describe each subcomponent of the PSM.
224
225 ***3.1 Variation in Coral Growth Rates***

226 Sub-seasonal resolution is a goal of many coral paleoclimate studies. However, a coral's growth rate
227 may vary both within and between years. For example, a *Porites* coral growing an average of 1.2
228 cm/year would achieve approximately monthly resolution if sampled in 1 mm increments. Although
229 monthly resolution is targeted, one sample of coral powder may average 2-3 weeks (-2σ) of time
230 when the coral is growing faster, or 5-6 weeks (+2σ) when the coral is growing slower. Due to variable
231 growth rates, the net effect of equal sampling in the depth domain will lead to unequal sampling in
232 the time domain. We use our coral PSM to assess how variations in coral growth impact the variance
233 of a resulting geochemical time series.
234

We measured the annual growth rates of 9 modern and fossil *Porites* cores from the southwest Pacific to generate a distribution of growth rates with a mean of 1.2 ± 0.2 cm/year (±1σ). The measured growth rate values are consistent with the reported average values for *Porites* corals from other regions of the Pacific [*Cobb et al.*, 2013]. We incorporate variable growth rates into the coral PSM using an autoregressive order 2, AR(2), model since the measured annual growth rates are serially correlated and cannot be modeled with an independent error term. The lag 1 and 2 correlation coefficients (0.25 and 0.20, respectively), and the standard deviation (0.2 cm/year) for the AR(2) model are based on measured *Porites* corals. The AR(2) model is used to generate a series of growth rates (Figure 2a). The distribution of simulated growth rates (Figure 2b) is consistent with the measured coral growth rates. The parameters for the AR(2) model can easily be adjusted for different species.

A realization of the AR(2) model provides a transformation from the time to the depth domain. One random realization for SST and forward modeled $\Delta\delta^{18}O_{pseudocoral}$ is provided at Christmas Island and Vanuatu as an illustrative example of how the algorithm works (Figure 3a-d). The net effect of the variable growth rate algorithm is that the pseudocoral output looks stretched and compressed relative to the original input. Monte Carlo methods are employed to generate many random realizations.

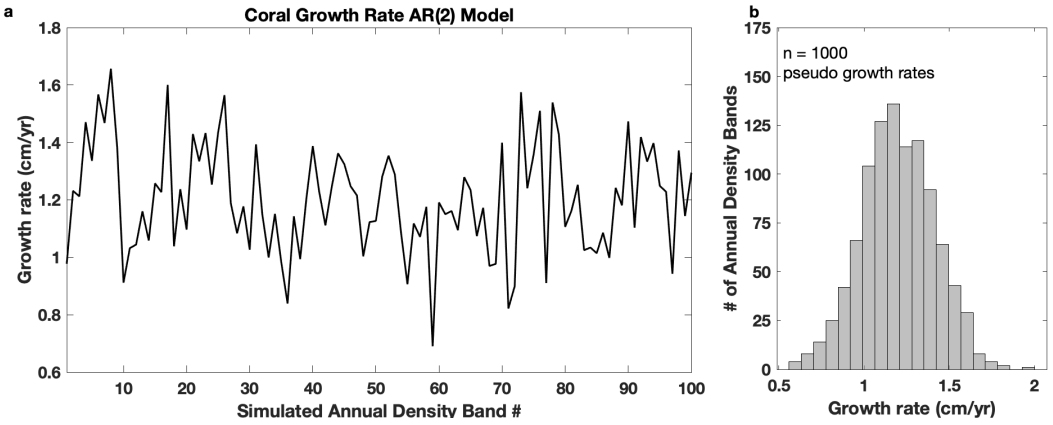

Figure 2. Simulated annual coral growth rates (cm/year). (**a**) A randomly generated realization of simulated growth rates for 100 pseudocoral annual density bands. The growth rates are simulated using an autoregressive order 2, AR(2), model with lag coefficients and variance parameters determined from measured *Porites* corals from the southwest Pacific (Section 3.1). Here we show one randomly generated realization of the AR(2) simulated growth rates, but note that the model can be run for *n* realizations. (**b**) Histogram of modeled pseudo *"Porites"* annual growth rates (1.2 ± 0.2 cm/year, ±1σ). The pseudocoral annual growth rates are used stretch and compress the environmental inputs to mimic how equal sampling in the depth domain can yield to unequal sampling in the time domain.

3.2 Analytical and Calibration Errors

Monte Carlo methods are also used to randomly generate 1000 $\Delta\delta^{18}O_{pseudocoral}$ and $SST_{Sr/Ca}$ time series perturbed with analytical and calibration errors modeled as Gaussian white noise (Figure 3e-h). For $\Delta\delta^{18}O_{pseudocoral}$, analytical errors are taken as 0.20‰ (±2σ), a value typical of laboratory analytical precision. For coral $SST_{Sr/Ca}$, we incorporate the combined effect of the analytical instrument error, as well as the linear calibration error associated with transforming coral Sr/Ca into SST. Previous work identified that that the net effect of analytical and calibration errors can cause uncertainties of ~0.30°C (±2σ) [*Alibert and McCulloch*, 1997; *Schrag*, 1999; *Quinn and Sampson*, 2002]. The original SST environmental inputs are thus perturbed with Gaussian white noise that includes the combined impact of analytical and calibration errors (0.30°C, ±2σ). The error term for $SST_{Sr/Ca}$ can be changed

within the PSM framework to account for larger analytical and calibration error terms that have been previously reported [*Corrège*, 2006; *DeLong et al.*, 2013; *Hathorne et al.*, 2013; *Sayani et al.*, 2019].

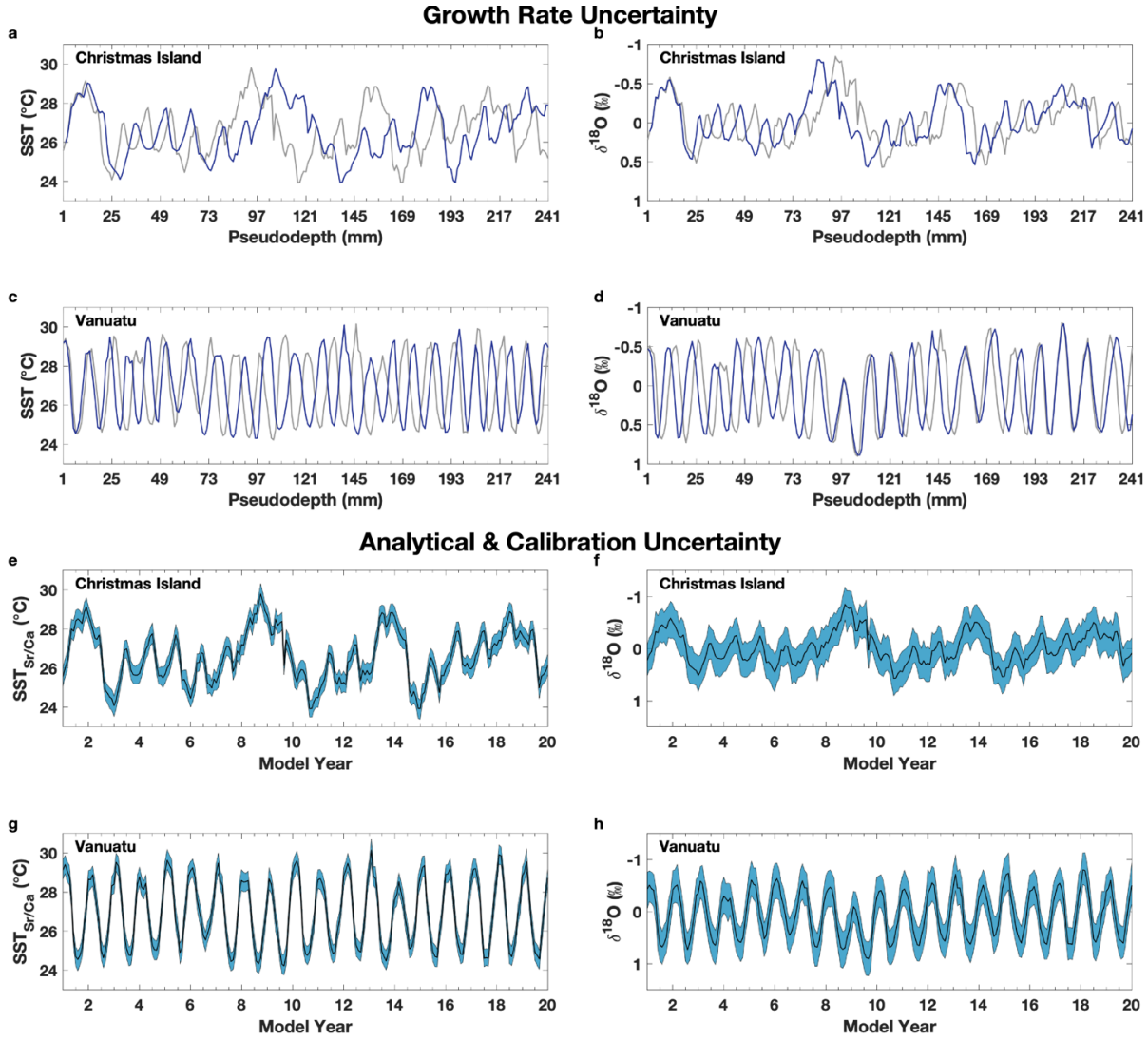

Figure 3. Impact of variable growth rates and analytical and calibration errors on environmental signals. (**a-d**) Blue curves depicts the original SST (**a, c**) and $\Delta\delta^{18}O_{pseudocoral}$ (**b, d**) inputs transformed from the time to the depth domain using a realization of the AR(2) variable growth rate model. Gray curves indicate the original inputs transformed to the depth domain using a constant transformation of 1.2 cm/year (i.e., no variable growth rates) for the model grid points closest to Christmas Island (**a, b**) and Vanuatu (**c, d**). Model output in this and all subsequent figures are from the CESM-LME 850 control [*Otto-Bliesner et al.*, 2016] (Section 2.1). $\Delta\delta^{18}O_{pseudocoral}$ in this and all subsequent figures is generated using the sensor model of *Thompson et al.* [2011] (Section 2.2.1). (**e, g**) Pseudocoral $SST_{Sr/Ca}$ perturbed with the combined effect of analytical and calibration errors (±0.30°C, 2σ; Section 3.2) at the model grid points closest to Christmas Island (**e**) and Vanuatu (**g**). (**f, h**) $\Delta\delta^{18}O_{pseudocoral}$ perturbed with analytical error (±0.20‰, 2σ; Section 3.2) for Christmas Island (**f**) and Vanuatu (**h**). Black line in (**e-h**) indicates the unperturbed environmental inputs for the selected sites, and the blue shading represents the spread of forward modeled pseudocoral time series (n = 1000). For clarity, each panel includes a 20-year subset of the 850 control to show how variable growth rates and analytical/calibration errors impact the original inputs.

3.3 Monthly Coral Chronology

The creation of an age model in coral paleoclimate studies often requires the measured climate indicator (proxy) be transformed from the depth into the time domain. We investigate the impact of

key age modeling assumptions on interannual variance. We note that the assumptions discussed here are different than the uncertainties that arise from missing or double counting years in annually banded archives [*Comboul et al.*, 2014] that have been previously incorporated into existing PSM frameworks [*Dee et al.*, 2015].

The chronology for approximately monthly-resolved coral data typically uses annual cyclicity in the data and the summer and wintertime extremes to constrain a relative chronology. For coral Sr/Ca, larger values indicate cooler temperatures, while smaller values indicate warmer temperatures [*Weber*, 1973; *Smith et al.*, 1979; *Beck et al.*, 1992]. For coral $\delta^{18}O$, more negative extrema indicate warmer and/or fresher conditions often experienced during the summer, while more positive extrema indicate cooler and/or more saline conditions experienced during the winter [*Fairbanks et al.*, 1997; *Corrège*, 2006; *Lough*, 2010]. Peaks and troughs identified in the geochemical data are assigned a calendar month based on knowledge about the climatology at a given site, and then the data is interpolated to achieve monthly resolution. The relative age model can be further refined by overlapping the coral record with instrumental observations (modern corals only) and with high-precision ^{230}Th ages that serve as absolute chronological constraints with errors ~1% of the age [*Shen et al.*, 2012; *Cheng et al.*, 2013].

We developed a publicly available MATLAB® algorithm to standardize coral age modeling. The age-model algorithm assumes optimal sampling [*DeLong et al.*, 2013] of the coral at sub-seasonal resolution. Input variables include the estimated sampling resolution (e.g., 10-14 samples per annual growth band), the target temporal resolution (defaults to 12 points/year), and the climatological warmest and coldest months at a given location. The climatological warmest/coldest month assignment can be determined from instrumental observations or model output for past time intervals when the annual cycle is not known. The algorithm identifies peaks and troughs in the geochemical data that are then assigned a particular calendar month based on the climatological input. The algorithm also contains an option to constrain the number of years based on an approximate number of annual density bands visible in a coral's X-ray image. The number of years constraint is often not necessary for sites with a clear annual cycle (e.g., the southwest Pacific), but may be necessary for sites with a small and/or noisy annual cycle (e.g., the equatorial Pacific). Once an optimal number of peaks/troughs are iteratively identified, the geochemical data is interpolated to the target resolution using a piecewise linear transformation [*Fritsch et al.*, 1980].

We apply the age model algorithm to assess the impact on interannual variance using SST from the grid points nearest to Vanuatu and Christmas Island (Figures 4-5; see Supporting Figures 1-2 for $\Delta\delta^{18}O_{pseudocoral}$). Simulated SST at Vanuatu shows a clear annual cycle with the climatological warmest month occurring in February (coldest in August) (Figure 4a). The algorithm does well in identifying summer and winter in Vanuatu (Figure 4c), but at Christmas Island, where the annual cycle is smaller (Figure 5a) the algorithm encounters more difficulties in identifying seasonal extrema due to the relatively large amplitude of interannual variability (Figure 5b). Uncertainty in the age model of a coral record results when a common assumption in coral age modeling that the climatological warmest/coldest months do not change is violated.

To show how this uncertainty manifests, we show the spread in the distribution of warmest/coldest months. The spread in the distribution of summer/winter months at Vanuatu (Figure 4b) is narrow, so the algorithm has more success in identifying the correct calendar month in the extrema in the timeseries. That said, there is still incorrect month assignment in the age model. For example, March is the actual warmest month in model year 4, but the age model algorithm assigns the month of

February to the SST peak (Figure 4c). In contrast, the distribution of warmest/coldest months at Christmas Island (Figure 5b) is broad, so there is much more error in assigning the correct calendar month to extrema. In worst-case scenarios, model years with strong El Niño events have a small, nearly absent annual cycle with SSTs during boreal winter surpassing the climatological summertime maximum values. Without constraining the approximate number of years, it is easy to miss weak troughs during boreal winters with El Niño events, and therefore years. These age model assumptions can yield large differences (~10-30%) in interannual variance when the climatology of the age modeled time series (Figure 5d, 5f) is removed to generate SST anomalies (Figure 5g).

Our age-model algorithm is deterministic, meaning that for a given Sr/Ca or $\delta^{18}O$ input series the age model will iteratively find a single solution that meets the constraints provided by the user. In the context of the full coral PSM presented here, multiple realizations of age modeled pseudocoral output can be generated by first perturbing the PSM input with the variable growth rate algorithm (Section 3.1). Alternatively, the user can follow the protocol of the *Comboul et al.* [2014] banded age model and perturb the number of years constraint within error.

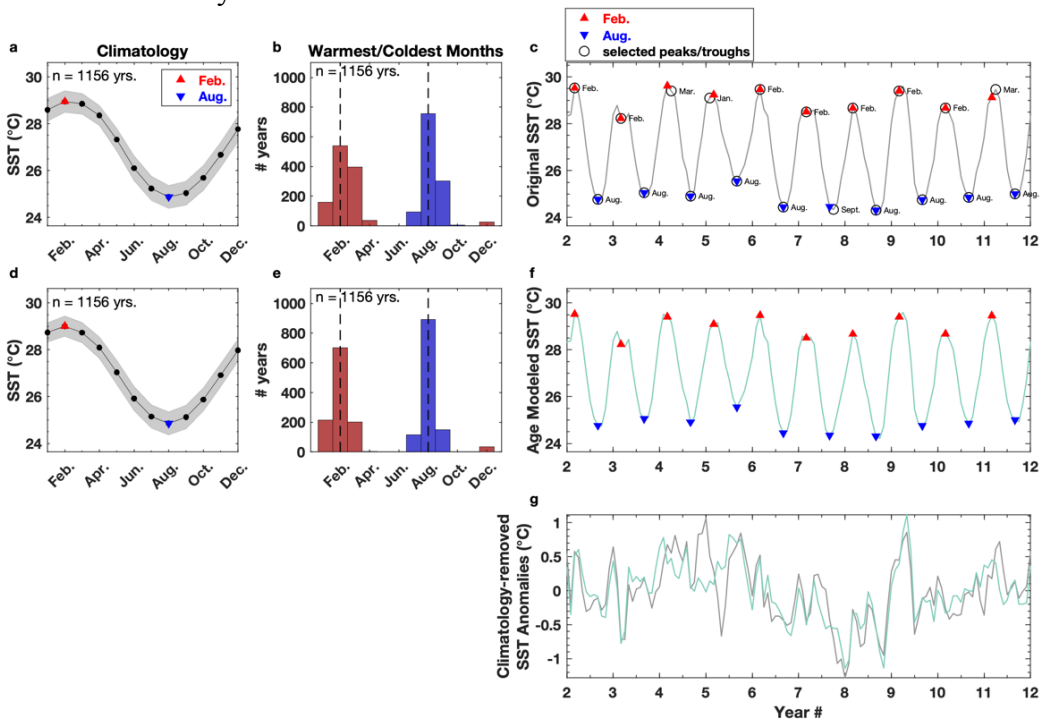

Figure 4. Age modeling of pseudocoral SST at Vanuatu. Climatology (black) ± 1σ (shading) for the original (**a**) and age modeled (**d**) SST output for the grid point nearest Vanuatu in the LME 850 control (n = 1156 years). Histogram of the warmest (red bars) and coldest (blue bars) month for each individual year in the 850 control (**b**) and the age modeled SST output (**e**). The climatological warmest/coldest months (dashed vertical lines) do not always equal the actual warmest/coldest month in each year. 10 years of the original monthly SST (**c**, gray line) and age modeled SST (**f**, teal line). Triangles in (**a, c, d, f**) indicate the climatological warmest (Feb.) and coldest (Aug.) months. The black circles in (**c**) indicate the peak/troughs identified by the age model algorithm, and the adjacent text labels indicate the calendar month at each critical point. The critical points in (**c**) are assigned the climatological warmest (Feb.) and coldest (Aug.) months, and the data is linearly interpolated in between the critical points to generate the age modeled time series in (**f**). The triangle markers in (**f**) better line up with the actual peaks and troughs in the age modeled time series compared to the original environmental input in (**c**). (**g**) Monthly SSTA for the original input (black) and age modeled pseudocoral SST (teal). In this and all subsequent figures, anomalies are with respect to the climatology of the full-length control run. The warmest/coldest month distributions in (**b**) and (**e**) are wider than a single month, and is directly related to the loss of interannual variance in (**g**).

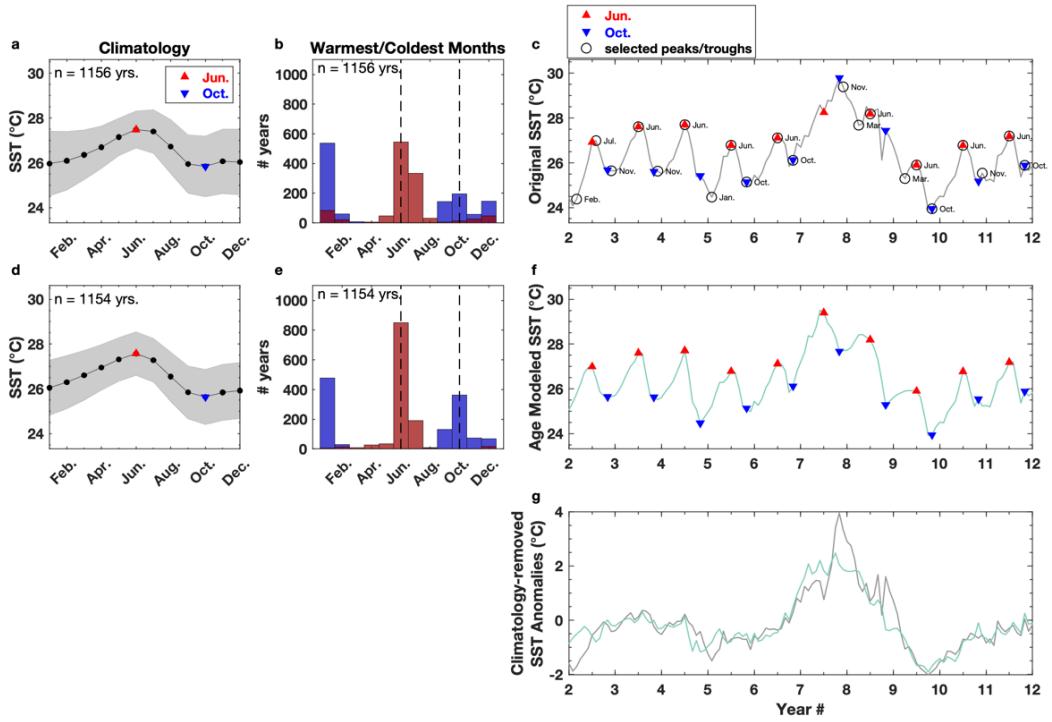

Figure 5. Age modeling of pseudocoral SST at Christmas Island. Same as Figure 4 except for the grid point nearest to Christmas Island. Triangles in (**a, c, d, f**) indicate the climatological warmest (Jun.) and coldest (Oct.) months. Years with strong El Niño events (e.g. model years 8 and 9) have a reduced annual cycle and a small and/or absent trough during boreal winter, leading to incorrect month assignment in (**f**) and a reduction in interannual variance in (**g**).

4. Results & Discussion

Our coral PSM quantifies how analytical and calibration errors, variable growth rates, and age modeling assumptions transduce input climate signals and impact interannual variance, and subsequently estimates of ENSO variability. Tropical reefs are point sources for paleoclimate reconstructions; whereas, with climate model output we can advantageously run the coral PSM at every grid point in the tropical Pacific to identify regional patterns. Broad regions of the tropical Pacific exhibit distinct patterns when the original environmental inputs are perturbed using the coral PSM. We separate the identified patterns into three sections: changes in the standard deviation of monthly anomalies as recorded by corals, decadal and longer changes in ENSO variability, and decadal and longer changes in ENSO variability as recorded by corals.

4.1 Quantifying Changes in Interannual Variability: Monthly Standard Deviation

The percent change in standard deviation between the perturbed pseudocorals and the original SST or $\Delta\delta^{18}O_{pseudocoral}$ climatology-removed anomalies is a method used to quantify changes in variance. The percent change (Figure 6) is calculated using the median standard deviation value for *n* realizations of the perturbed pseudocoral monthly anomaly time series, and highlights site dependencies in the results. The changes in interannual variance between the original environmental inputs and the coral PSM output at a given location is linked to both the amplitude of the interannual signal and the annual cycle. Analytical and calibrations errors (Section 3.2) cause a systematic increase in interannual variance for pseudocoral $SST_{Sr/Ca}$ (Figure 6b) and $\Delta\delta^{18}O_{pseudocoral}$ (Figure 6f) compared to the original environmental inputs. Regions of the Pacific with a large interannual signal

(Figure 6a, 6e) are less impacted by analytical/calibration errors compared to regions with a smaller interannual signal.

The increase in annual cycle regularity induced by the age model (Section 3.3) broadly tends to cause a decrease in interannual variance across most of the tropical Pacific (Figure 6d, 6h). The largest percent change in standard deviation occurs in the central Pacific and eastern Pacific cold tongue regions where ENSO events can lead to climatological coldest months that are warmer than the climatological warmest months. It is thus difficult to identify a trough in the geochemical data and accurately assign a month to the data when age modeling (Section 3.3). The age model effects are particularly exacerbated in the CESM-LME due to biases in the amplitude of ENSO events [*Otto-Bliesner et al.*, 2016]. Conversely, pseudocorals at sites with a larger annual cycle and less variable distribution of warmest and coldest months have a smaller reduction in interannual variance compared to the original environmental input (Figure 6d, 6h). Outside of the tropics, however, sites that have multiple consecutive months with approximately the same average SST value experience an increase in variance (Figure 6d). For a given site, the magnitude of the percent change is typically larger for $\Delta\delta^{18}O_{pseudocoral}$ compared to SST given that $\delta^{18}O$ is multivariate and may have contributions from SSS that may be a few months out of phase with SST [*Gorman et al.*, 2012] (Figure 6d versus 6h).

The percent change in standard deviation for the full coral PSM (Figure 7) reveals the tradeoff between interannual variability and the amplitude of the annual cycle. At locations with the strongest interannual signal (equatorial sites), the loss of variance due to the age model assumptions exerts the dominant influence on interannual variance for pseudocoral $SST_{Sr/Ca}$ (Figure 7a) and $\delta^{18}O$ (Figure 7b). Although age model uncertainty also causes a decrease in variance in regions like the southwest Pacific, the relative magnitude of the change is compensated by the increase in variance that results from analytical and calibration errors. Our results highlight that the different processes and assumptions inherent to coral-based studies exert sizable impacts on pseudocoral interannual variance, and that the relative contributions are site dependent. While changes in the monthly standard deviation of an individual anomaly time series can show longer term changes in ENSO [*Wittenberg*, 2009], uncertainties in coral climate reconstructions [*Emile-Geay et al.*, 2013a; 2013b] preclude such a reconstruction back in time, thus warranting an alternative metric for paleo-ENSO studies.

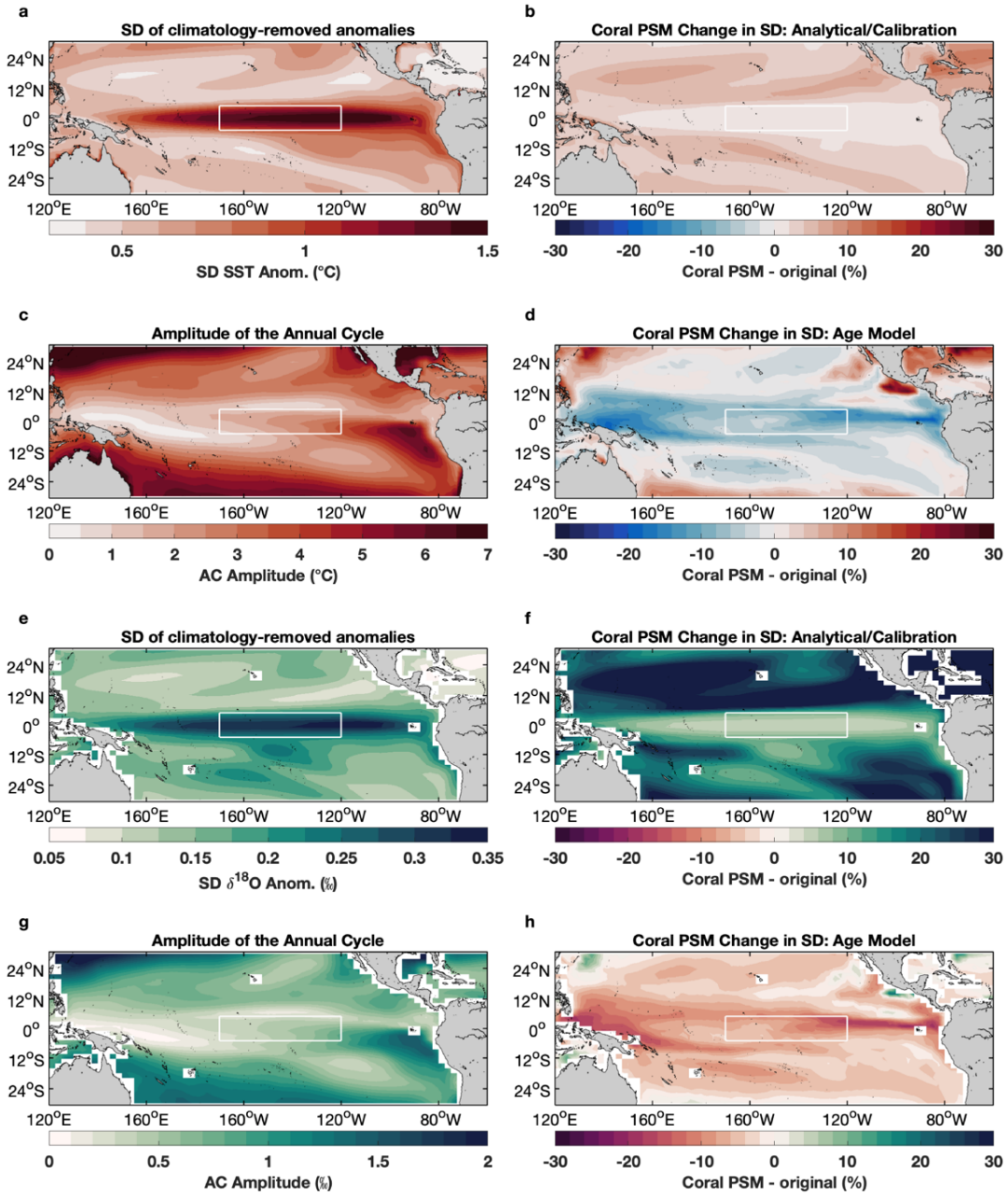

Figure 6. Pseudocoral $SST_{Sr/Ca}$ and $\delta^{18}O$ changes in interannual variance. (**a**) Standard deviation (SD) of monthly SSTA in the LME 850 control. Warm colors highlight regions with the largest interannual signal. (**b**) Percent change in SD between pseudocoral $SST_{Sr/Ca}$ anomalies perturbed with analytical and calibration errors and the SD of the unperturbed SST anomalies. (**c**) Amplitude of the annual SST cycle in the LME 850 control. (**d**) Percent change in SD between age modeled pseudocoral $SST_{Sr/Ca}$ anomalies and the original, unperturbed SST anomalies. (**e**) SD of monthly forward modeled $\Delta\delta^{18}O_{pseudocoral}$. (**f**) Percent change in SD between pseudocoral $\delta^{18}O$ anomalies perturbed with analytical errors and the SD of the unperturbed $\Delta\delta^{18}O_{pseudocoral}$ anomalies. (**g**) Amplitude of the annual $\Delta\delta^{18}O_{pseudocoral}$ cycle in the 850 control. (**h**) Percent change in SD between age modeled pseudocoral $\Delta\delta^{18}O$ anomalies and the original, unperturbed $\Delta\delta^{18}O$ anomalies. The percent change in SD for the full-length time series (~1156 years) is reported. The SD for the coral PSM output is the median of 1000 realization in (**b, f**) and 1 realization of the deterministic age model (**d, h**). Colormaps in this and all subsequent maps use the cmocean: colormaps for oceanography toolbox [*Thyng et al.*, 2016]. The Niño 3.4 region is outlined by a white box (**a-h**). The changes in interannual variance from analytical/calibration errors (**b, f**) is related to the amplitude of the interannual signal (**a, e**), whereas the change in variance from age modeling (**d, h**) is linked to the amplitude of the annual cycle (**c, g**).

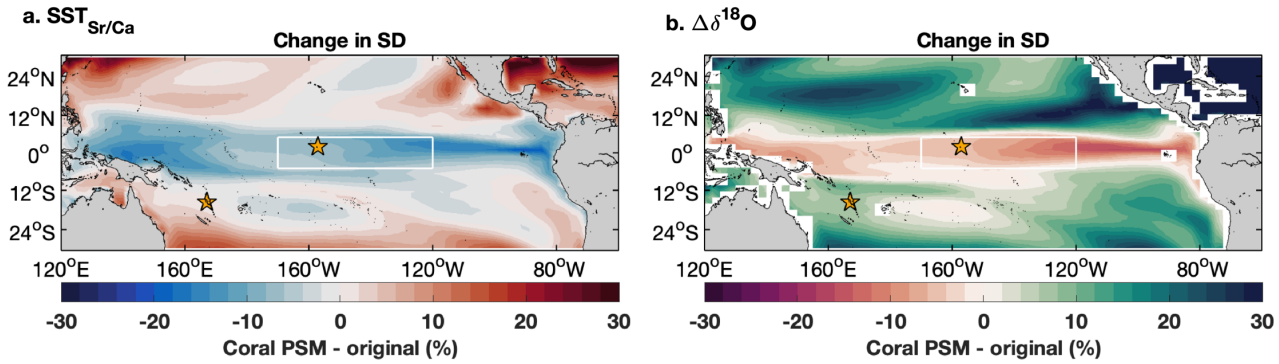

Figure 7. Changes in interannual variance for the full coral PSM. Percent change in SD between pseudocoral $SST_{Sr/Ca}$ (**a**) and $\Delta\delta^{18}O$ (**b**) anomalies perturbed with variable growth rates, analytical/calibration errors, and the age modeling algorithm, and the original, unperturbed environmental input (n = 100 realizations). Selected sites at Christmas Island (2°N, 157°W) in the central Pacific, and Vanuatu (16°S, 167°E) in the southwest Pacific are indicated with gold stars. The white box outlines the Niño 3.4 region. The percent change in SD for the full coral PSM reveals the tradeoff between interannual variability and the amplitude of the annual cycle (Figure 6).

4.2 Quantifying Changes in ENSO Variability: Decadal+

Although precise month-to-month variations of SST in the Niño 3.4 region are a sought-after target for ENSO studies, this is difficult to reconstruct back in time using a limited number of coral proxy records with age uncertainties. Previous studies have used sophisticated statistical techniques on corals from the last millennium and still had an appreciable degree of uncertainty in the reconstruction [*Emile-Geay et al.*, 2013a; 2013b]. Fossil corals with absolute age errors on the order of 1% make a month-to-month reconstruction virtually impossible on 10^3 year and longer timescales. We address this challenge by building upon the procedure suggested in *Trenberth* [1997] and use descriptive statistics and probability theory to quantify changes in ENSO variability on the timescale of decades. Indeed, the technique of looking at changes in ENSO over windows in the past has already been employed using corals from the central Pacific [*Cobb et al.*, 2013]. In this sub-section, we formalize the technique to quantify changes in ENSO in reconstructions and then couple it to the coral PSM in Section 4.3.

We demonstrate different methods of quantifying changes in ENSO variability using climatology-removed SST anomalies averaged across the Niño 3.4 region (Figure 6, box) as an illustrative example to show how the different techniques all agree on the changes in ENSO, but have different applicability. We restrict the time series (Figure 8a) to the first 200 years purely for discussion purposes in this section but use the entire control run for the remainder of the analyses. During El Niño (La Niña) events, the Niño 3.4 region experiences positive (negative) SST anomalies that peak during boreal winter while the western Pacific experiences negative (positive) excursions [*Trenberth*, 1997]. Strong El Niño and La Niña events yield SST anomalies that fall into the tails of the SSTA distribution (Figure 8b, 8c). An increase in the frequency and/or magnitude of strong ENSO events will increase the width of the SSTA distribution, and result in a larger standard deviation. This technique works best on data that has small uncertainty in the time domain or in the interpretation.

Here we introduce a calculation to quantify fluctuations in SSTs from the Niño 3.4 region on decades or longer timescales, as these changes are more readily captured in paleo-ENSO reconstructions using archives with uncertainties. Longer-term changes in the amplitude and frequency of large SST anomalies can occur for decades or longer intervals, which we call decadal+ variability. As an example of the types of changes that this technique captures, model years 100-120 (Figure 8a) has

smaller amplitude SSTA compared to the frequent large amplitude anomalies in model years 125-150. These changes occur in the absence of external forcing, as this is an unforced model simulation, and they likely result from complex interactions between ENSO and other internally driven modes of variability [*Wittenberg*, 2009; *Wittenberg et al.*, 2014; *Sun and Okumura*, 2019]. We quantify decadal+ changes in ENSO *variability* using the running standard deviation of climatology-removed monthly SSTA of 20-year windows averaged across the Niño 3.4 region ($\sigma_{\text{Niño3.4-SSTA}}$; Figure 8d) [*Okumura et al.*, 2017]. Here we use a 20-year running standard deviation as many fossil coral record lengths are short, but our approach is applicable to investigating changes in variability over longer time intervals. Larger $\sigma_{\text{Niño3.4-SSTA}}$ values indicate increased ENSO variability, whereas smaller $\sigma_{\text{Niño3.4-SSTA}}$ values indicate decreased ENSO variability during a time interval. The wide range of internal ENSO variability within the CESM-LME 850 control is reflected in the width of the $\sigma_{\text{Niño3.4-SSTA}}$ distribution (Figure 8e, 8f). We posit that longer term, decadal+ changes in ENSO variability, as reflected by $\sigma_{\text{Niño3.4-SSTA}}$ and the distribution of standard deviation values (Figure 8f), is a feasible target for coral-based paleoclimate reconstructions since this metric reduces the influence of uncertainties, especially temporal.

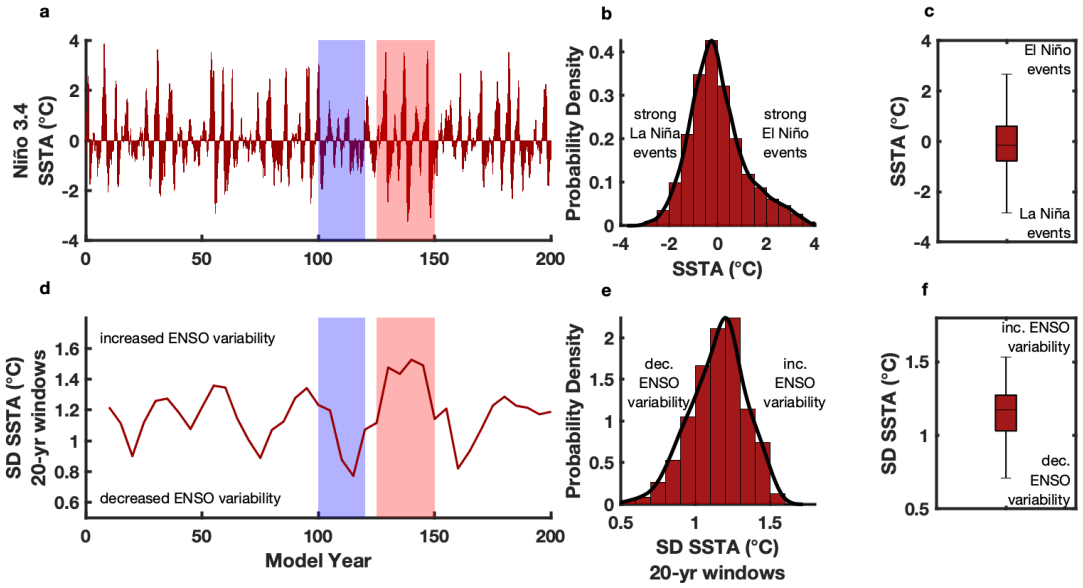

Figure 8. Quantifying changes in internal ENSO variability. (**a**) Monthly SSTA averaged across the Niño 3.4 region in the 850 control (200-yr subset shown for clarity). Distribution of Niño 3.4 SSTA depicted as a histogram/PDF (**b**) and box plot (**c**) for the full-length control (1156 years). (**d**) 20-yr running standard deviation of Niño 3.4 monthly SSTA ($\sigma_{\text{Niño3.4-SSTA}}$). Shaded portions in (**a, d**) highlight two intervals with more (red) and less (blue) internal ENSO variability. Distribution of $\sigma_{\text{Niño3.4-SSTA}}$ values depicted as a histogram/PDF (**e**) and box plot (**f**). Higher SD values indicate increased ENSO variability, whereas lower SD values indicate decreased variability. PDFs in (**b, e**) are based on a kernel density estimation method [*Parzen*, 1962]. The lower and upper bounds of the boxes in (**c, f**) correspond to the 25th and 75th percentiles and the center line indicates the median. The whiskers in (**c, f**) represent the 1.5 x inter-quartile range (IQR). Outliers greater than 1.5xIQR are omitted for clarity. The running SD of monthly anomalies (**f**) is a metric for decadal+ changes in interannual variability.

4.3 Quantifying Changes in ENSO Variability using Corals: Decadal+ with PSM

The coral PSM provides a tool to investigate how various uncertainties not only impact interannual variability locally, but also how the uncertainties broadly impact the ability of a pseudocoral to capture decadal+ changes ENSO variability. On interannual timescales, corals from circum-Pacific locations are influenced by ENSO, local variability, and how corals themselves records climate (Section 1). Our coral PSM addresses some of these confounding influences by quantifying how

analytical and calibration errors, variable growth rates, and age modeling assumptions modify input climate signals and impact interannual variance (Section 4.1). The running standard deviation of climatology-removed anomalies is presented as a more applicable metric in paleoclimate reconstructions for capturing temporal changes in interannual variability as well a means to provide constraints on the range of internal variability (Section 4.2). A running or windowed standard deviation is also advantageously poised to handle short (several decades or less) and/or discontinuous coral records, and has previously been employed for fossil coral records spanning thousands of years ago (the mid- to late-Holocene) [*Cobb et al.*, 2013].

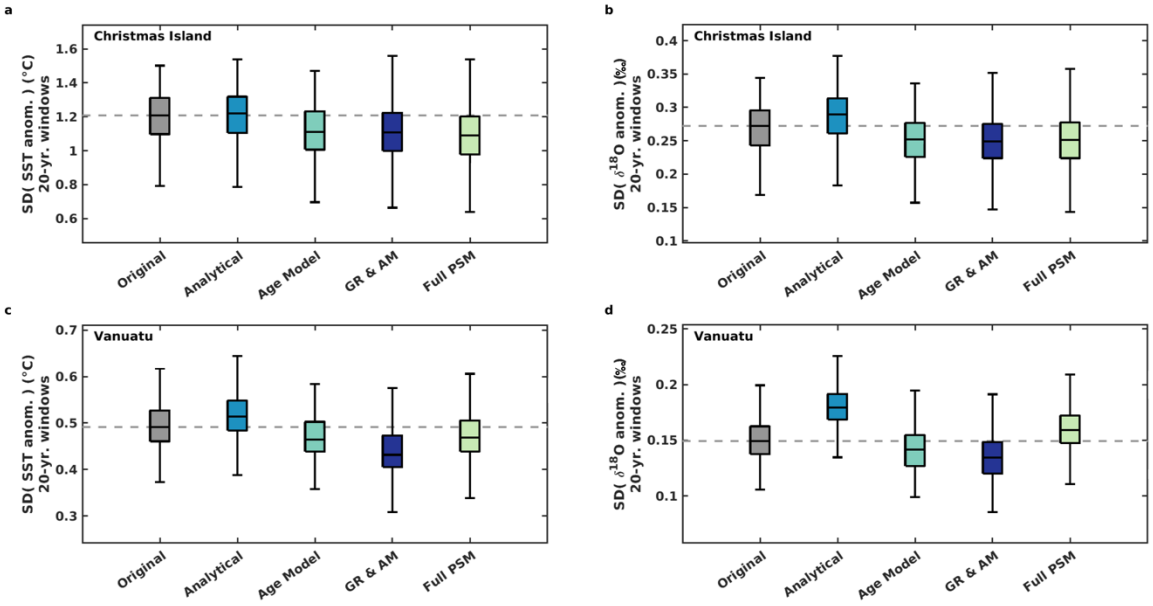

Figure 9. The impact of coral PSM uncertainties on interannual variance. Box plots showing the distribution of 20-yr running standard deviation values for pseudocoral $SST_{Sr/Ca}$ (**a, b**) and $\delta^{18}O$ (**c, d**) anomalies across all pseudocoral realizations for the Christmas Island (**a, c**) and Vanuatu (**b, d**) grid points. The growth rate and age model (GR & AM), analytical/calibration, and full PSM include the results for 1000 realizations. The deterministic age modeled results are shown for 1 realization. The full PSM is determined by consecutively running the growth rate algorithm, applying analytical/calibration error, and then age modeling all 1000 pseudocoral $SST_{Sr/Ca}$ or $\Delta\delta^{18}O_{pseudocoral}$ realizations. The lower and upper bounds of the boxes correspond to the 25th and 75th percentiles and the center line indicates the 50th percentile. The whiskers represent 1.5xIQR. Outliers greater than 1.5 x IQR are omitted for clarity. Dashed horizontal gray lines indicate the median SD for the original environmental inputs. The median 20-year running standard deviation of $SST_{Sr/Ca}$ and $\Delta\delta^{18}O_{pseudocoral}$ anomalies illustrates how the various PSM subcomponents systematically increase or decrease interannual variance. The length of the box and whiskers encapsulates information about the range of simulated internal variability.

The 20-year running standard deviation of $SST_{Sr/Ca}$ and $\Delta\delta^{18}O_{pseudocoral}$ anomalies for Christmas Island and Vanuatu (Figure 9) confirms that the various PSM subcomponents systematically impact interannual variance while also encapsulating information about the range of simulated internal variability. As with Niño 3.4 monthly SSTA (Figure 8f), the median standard deviation value of the original environmental inputs (Figure 9 gray boxes) indicates the overall amplitude of interannual variance at a site, whereas the height of the box and whiskers indicate the degree of internal variability. Christmas Island expectedly has a higher median standard deviation value and a larger spread compared to Vanuatu given that the site experiences larger interannual SST (Figure 6a) and $\delta^{18}O$ (Figure 6e) signals. Perturbing the original SST and $\Delta\delta^{18}O_{pseudocoral}$ time series at Christmas Island and Vanuatu with analytical and calibration errors (Section 3.2) systematically increases interannual variance (Figure 9 light blue) as quantified by the shift in the median standard deviation

value compared to the original environmental inputs. Incorrect assumptions about the timing of the warmest and coldest month assignment in the age model (Section 3.3) decreases interannual variance (Figure 9 teal). We do not isolate the impact of variable growth rates as the algorithm generates a "pseudodepth" vector (Section 3.1) that is not readily subset into 20-year windows. Instead, the original environmental input is perturbed with variable growth rates and then processed by the age model algorithm to generate multiple realizations (Figure 9 dark blue). The combined influence of variable growth rates and the age model assumptions causes a systematic decrease in interannual variance at both sites.

Although each individual sub-model of the PSM causes a systematic change in interannual variance at both Christmas Island and Vanuatu, the relative increase or decrease in the interannual signal (median standard deviation) for the full PSM, or the summation of the effects from the sub-components, is site dependent. These site dependencies are revealed when expanding the pseudocoral network to the entire tropical Pacific (Figure 10). For similar reasons discussed in section 4.1, the interannual variance change is closely related to the tradeoff between the magnitude of the interannual cycle and the amplitude of the annual cycle.

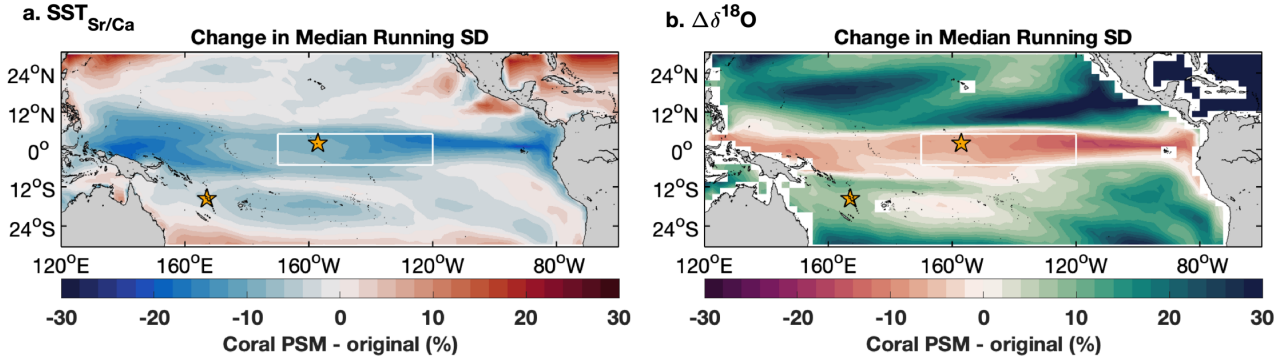

Figure 10. Changes in interannual variance for the full coral PSM. Percent difference in the median 20-year running standard deviation between pseudocoral $SST_{Sr/Ca}$ (**a**) and $\Delta\delta^{18}O$ (**b**) anomalies perturbed with variable growth rates, analytical/calibration errors, and the age modeling algorithm, and the original, unperturbed environmental input (n = 100 realizations). Gold stars indicate select sites at Christmas Island and Vanuatu. The white box indicates the Niño 3.4 region. The percent change in standard deviation for the full coral PSM reveals the tradeoff between interannual variability and the amplitude of the annual cycle. The patterns displayed here are similar to those of Figure 6, indicating that the two variability metrics yield consistent results.

We correlate Niño 3.4 SSTA with the pseudocoral realizations to demonstrate how corals from locations around the tropical Pacific record changes in ENSO, and begin with the familiar month-to-month calculation. The correlation of local SST or SSS anomalies with Niño 3.4 SSTA is canonically used to demonstrate the ENSO sensitivity at a site. A consistent pattern of response over the 1156-year-long control is an inverse temperature relationship between the central/eastern and western tropical Pacific with monthly SSTA from the Niño 3.4 region (Figure 11a). Forward modeled monthly $\Delta\delta^{18}O_{pseudocoral}$, a function of SST and SSS, also covaries with Niño 3.4 SSTA (Figure 11b) with the same pattern of response as SSTA (Figure 11a). For example, during El Niño events the central and eastern Pacific experience negative $\Delta\delta^{18}O_{pseudocoral}$ anomalies indicating the combined impact of warmer and fresher conditions, while the western Pacific experiences positive $\Delta\delta^{18}O_{pseudocoral}$ excursions indicative of colder and more saline conditions [*Fairbanks et al.*, 1997]. As previously discussed, the month-to-month correlation with Niño 3.4 SSTA is more applicable for observations or model output with no uncertainty in the time domain. Some of the uncertainties in coral proxy data

589 can be circumvented by instead shifting the focus to the ability of a coral to capture ENSO variability
590 on decadal+ timescales (Section 4.2).
591
592 Unlike the month-to-month maps, Niño 3.4 SSTA and the running standard deviation of $SST_{Sr/Ca}$ and
593 $\Delta\delta^{18}O_{pseudocoral}$ anomalies on decadal+ timescales are positively correlated across much of the tropical
594 Pacific (Figure 11c, 11d). The boomerang-shaped monthly SSTA correlation pattern that
595 distinguishes the western Pacific from the central/eastern Pacific (Figure 11a) essentially disappears
596 when examining how different regions of the Pacific track decadal+ changes in ENSO variability. In
597 the decadal+ calculation of ENSO variability, a significant positive correlation coefficient between
598 $\sigma_{Niño3.4\text{-}SSTA}$ and the running standard deviation of monthly SST (Figure 11c) or $\Delta\delta^{18}O_{pseudocoral}$ (Figure
599 11d) anomalies indicates that when ENSO variability increases or decreases in the Niño 3.4 region,
600 interannual variability at a given location tends to pace with those changes. The correlation with
601 $\sigma_{Niño3.4\text{-}SSTA}$ for the pseudocorals perturbed by the full coral PSM are expectedly smaller than the
602 original PSM inputs, but importantly, the temporal relationship with changes in SST variability in the
603 Niño 3.4 region is broadly preserved for both pseudocoral $SST_{Sr/Ca}$ (Figure 11e) and $\Delta\delta^{18}O_{pseudocoral}$
604 (Figure 11f) at many localities spanning the tropical Pacific despite all of the calculated coral
605 uncertainties. This highlights the strength of corals in their ability to capture decadal+ changes in
606 ENSO variability.

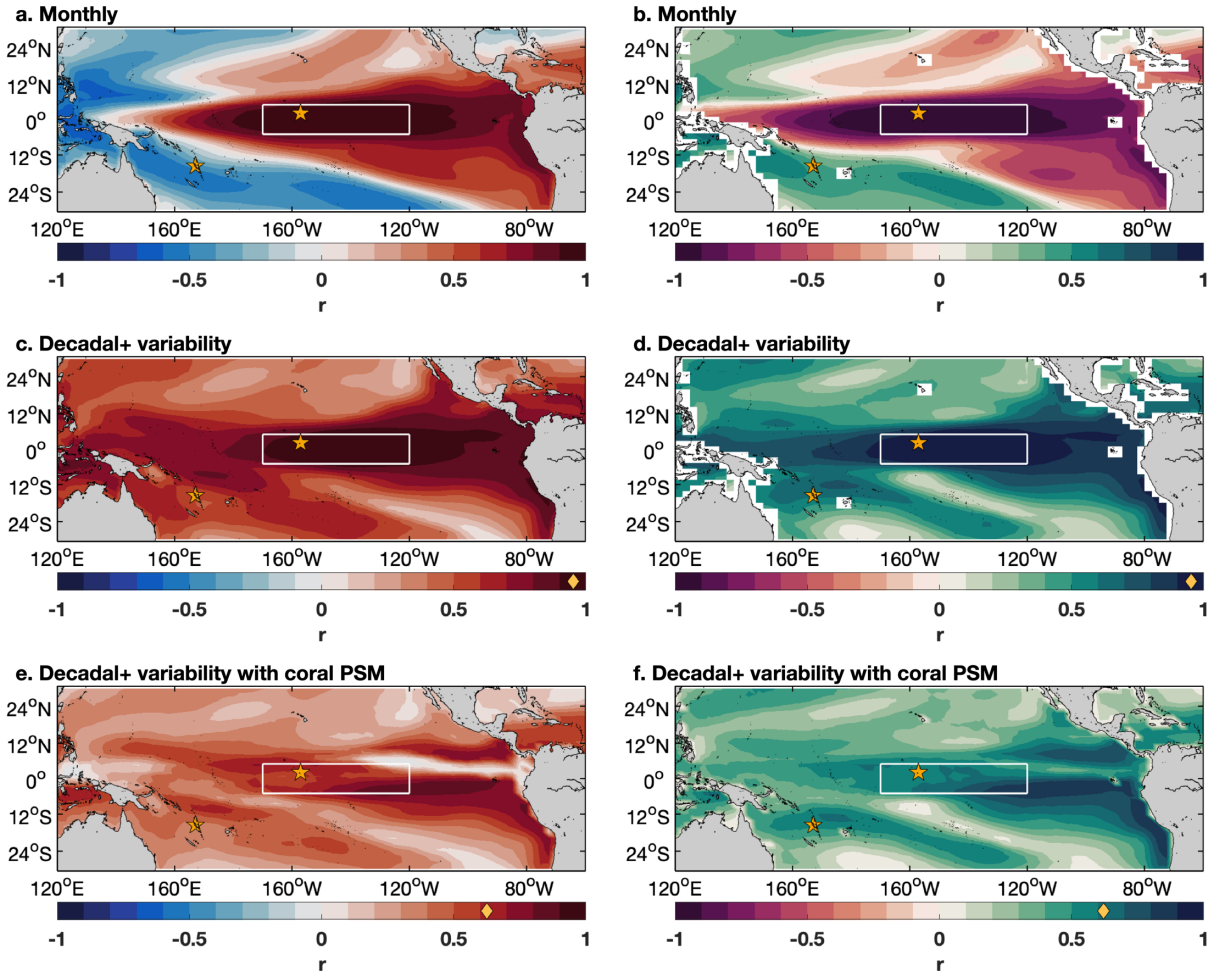

Figure 11. Correlation between Niño 3.4 SSTA and values at each grid point. Monthly Niño 3.4 correlated with monthly values for SSTA (**a**) and monthly values of forward modeled pseudocoral $\Delta\delta^{18}O_{pseudocoral}$ (**b**). The 20-yr running SD of Niño 3.4 SSTA ($\sigma_{Niño3.4\text{-}SSTA}$) with the 20-yr running SD of SSTA (**c**) and $\Delta\delta^{18}O_{pseudocoral}$ anomalies (**d**). The 20-yr running SD of Niño 3.4 SSTA with the 20-yr running standard deviation of SSTA (**e**) and $\Delta\delta^{18}O_{pseudocoral}$ anomalies (**f**) perturbed by the full coral PSM. Colormap in (**e, f**) is the median correlation coefficient for 100 full PSM realizations. The Niño 3.4 region is outlined by a white box (**a-f**). The correlation coefficient averaged across all grid points within the Niño 3.4 region (white box) is indicated with a gold diamond in (**c-f**). Colormaps provide the Pearson correlation coefficient [*Pearson*, 1920]. $\Delta\delta^{18}O_{pseudocoral}$ is generated using the sensor model of *Thompson et al.* [2011] (Section 2.2.1). Gold stars indicate select sites at Christmas Island and Vanuatu. Decadal+ changes in forward-modeled interannual $SST_{Sr/Ca}$ and $\delta^{18}O$ variability are positively correlated with $\sigma_{Niño3.4\text{-}SSTA}$ across much of the tropical Pacific (**e, f**) even with the added uncertainties in our PSM, indicating that these processes do not obfuscate the target climate signal of decadal+ changes in ENSO variability.

6. Conclusions

The coral PSM presented here fundamentally advances our knowledge of how corals modify interannual climate signals and how they record changes in ENSO variability. This study builds upon previous work by adding new archive and observation sub-models to the full PSM framework in order to quantitatively estimate the impact of various non-climatic processes on interannual variance in the final coral time series. Constraining such information is crucial given that estimation of interannual variance is one of the primary applications of coral paleoclimatology. Our process-based coral PSM explicitly incorporates an archive-based model (variable growth rates) as well as age modeling assumptions that are used when generating a coral geochemical time series. This study applies the

new PSM framework to the CESM LME 850 control run, which serves as the environmental input. The long control run allows us to include the impact of internal variability in our analyses, which is not possible using the short instrumental record. Although we note that the PSM is equally equipped to handle observational data or other climate model output. Our tools and algorithms are publicly available to the broader community to facilitate the comparison of coral geochemical data and observational data or climate model output, as well as facilitate the reproducibility of our results, via a GitHub repository (https://github.com/lawmana/coralPSM).

Our results characterize and document the ability of pseudocorals to capture decadal and longer, which we call decadal+, changes in ENSO variability. Coral proxy records of past ENSO variability come from a suite of sites spanning the western, central, and eastern tropical Pacific, all of which have varying signal to noise ratios with respect to ENSO. In some regions of the tropical Pacific, the combination of different uncertainties can increase or decrease interannual $SST_{Sr/Ca}$ and $\delta^{18}O$ variance by 10-30% (Figures 7 and 10). Our major conclusions are:

1. Analytical and calibration errors systematically increase interannual variance
2. Seasonal chronological uncertainties associated with transforming coral geochemical data from the depth to the time domain acts to decrease interannual variability
3. Variable growth rates in conjunction with age modeling assumptions decreases interannual variance
4. The change in interannual variance at a given location is related to the interannual signal and the amplitude of the annual cycle

Given that different processes exert sizable impacts on interannual variance, it is therefore most appropriate to compare coral geochemical data with instrumental observations or climate model output processed through this PSM. Nevertheless, despite the three uncertainties investigated in this study, the temporal relationship with changes in SST variability in the Niño 3.4 region is preserved for both pseudocoral $SST_{Sr/Ca}$ (Figure 11e) and $\Delta\delta^{18}O_{pseudocoral}$ (Figure 11f). Importantly, decadal+ changes in forward-modeled interannual $SST_{Sr/Ca}$ and $\delta^{18}O$ variability are positively correlated with $\sigma_{Niño3.4\text{-}SSTA}$ across much of the tropical Pacific. Despite all of the added uncertainties in our PSM, these processes do not obfuscate the target climate signal of decadal and longer changes in ENSO variability. This increases confidence that despite these major sources of uncertainties investigated herein, coral geochemical records from across the tropical Pacific are useful tools to reconstruct changes in ENSO variability back in time.

Quantifying the range of ENSO variability experienced during different background climate states is critical as this can help constrain projections of how ENSO variability may change in the future with anthropogenic warming. Paleoclimate reconstructions serve as important out-of-sample tests of ENSO variability. The ability to characterize past and future changes in ENSO variability benefits from proxy system modeling studies such as this that incorporate information from both models and proxy records. By putting climate model output and proxy data on a level playing field, we can reconcile the agreement between climate models and proxy-inferred responses and take an important step toward predicting how ENSO will respond to future radiative forcing.

Acknowledgements

This research was supported by NSF grant #1805874 under the Paleoclimate Perspectives on Climate Change (P2C2) competition (to J.W.P) and the National Science Foundation Graduate Research Fellowship Program (to A.E.L). We thank Tim Shanahan and Rowan Martindale for their feedback

on manuscript. We also thank Anthony Krupa for helping A.E.L. measure the annual coral growth rates used to develop the parameters for the growth rate AR(2) model. We thank the members of the PAGES Data Assimilation and Proxy System Modeling (DAPS) community for their feedback at the May 2019 working group meeting.

Author Contributions

A.E.L led the project and wrote the manuscript. A.E.L generated the figures and interpreted the results with input and feedback from all authors. A.E.L and C.A.C developed the MATLAB® code for the growth rate, analytical/calibration, and age model algorithms for the coral PSM with initial counsel from S.G.D. T.M.Q, J.W.P., S.G.D., and P.D.N. provided regular feedback on the analysis and writing. J.W.P, S.G.D., and P.D.N contributed to the initial inception of the research ideas. All authors reviewed the manuscript.

Code Availability

The MATLAB® codes that have contributed to the analysis and results in this study are publicly available on the GitHub repository for the lead author (https://github.com/lawmana/coralPSM).

Additional Information

Supporting information is available for this paper.

Competing Financial Interests: The authors declare no competing financial interests.

References

Alibert, C., and M. T. McCulloch (1997), Strontium/calcium ratios in modern *Porites* corals from the Great Barrier Reef as a proxy for sea surface temperature: Calibration of the thermometer and monitoring of ENSO, *Paleoceanography*, *12*(3), 345–363, doi:10.1029/97PA00318.

Beck, J. W., R. L. Edwards, E. Ito, F. W. Taylor, J. Recy, F. Rougerie, P. Joannot, and C. Henin (1992), Sea-surface temperature from coral skeletal strontium/calcium ratios, *Science*, *257*(5070), 644–647, doi:10.1126/science.257.5070.644.

Bellenger, H., E. Guilyardi, J. Leloup, M. Lengaigne, and J. Vialard (2014), ENSO representation in climate models: from CMIP3 to CMIP5, *Clim Dyn*, *42*(7-8), 1999–2018, doi:10.1007/s00382-013-1783-z.

Bin Wang, X. Luo, Y.-M. Yang, W. Sun, M. A. Cane, W. Cai, S.-W. Yeh, and J. Liu (2019), Historical change of El Niño properties sheds light on future changes of extreme El Niño, *Proc Natl Acad Sci USA*, *116*(45), 22512–22517, doi:10.1073/pnas.1911130116.

Bjerknes, J. (1969), Atmospheric teleconnections from the equatorial pacific, *Mon. Weather Rev.*, *97*(3), 163–172, doi:10.1175/1520-0493(1969)097<0163:ATFTEP>2.3.CO;2.

Brown, J., A. W. Tudhope, M. Collins, and H. V. McGregor (2008), Mid-Holocene ENSO: Issues in quantitative model-proxy data comparisons, *Paleoceanography*, *23*(3), doi:10.1029/2007PA001512.

717 Cai, W. et al. (2014), Increasing frequency of extreme El Niño events due to greenhouse warming,
718 *Nature Climate Change*, *4*(2), 111–116, doi:10.1038/nclimate2100.

719 Cai, W. et al. (2015), Increased frequency of extreme La Niña events under greenhouse warming,
720 *Nature Climate Change*, *5*(2), 132–137, doi:10.1038/nclimate2492.

721 Cheng, H. et al. (2013), Improvements in ^{230}Th dating, ^{230}Th and ^{234}U half-life values, and U–Th
722 isotopic measurements by multi-collector inductively coupled plasma mass spectrometry, *Earth*
723 *Planet. Sci. Lett.*, *371-372*(C), 82–91, doi:10.1016/j.epsl.2013.04.006.

724 Cobb, K. M., N. Westphal, H. R. Sayani, J. T. Watson, E. Di Lorenzo, H. Cheng, R. L. Edwards,
725 and C. D. Charles (2013), Highly variable El Niño–Southern Oscillation throughout the
726 Holocene, *Science*, *339*(6115), 67–70, doi:10.1126/science.1228246.

727 Cole, J. E., R. G. Fairbanks, and G. T. Shen (1993), Recent variability in the Southern Oscillation:
728 Isotopic results from a Tarawa Atoll coral, *Science*, *260*(5115), 1790–1793,
729 doi:10.1126/science.260.5115.1790.

730 Collins, M. et al. (2010), The impact of global warming on the tropical Pacific Ocean and El Niño,
731 *Nature Geosci.*, *3*(6), 391–397, doi:10.1038/ngeo868.

732 Comboul, M., J. Emile-Geay, M. N. Evans, N. Mirnateghi, K. M. Cobb, and D. M. Thompson
733 (2014), A probabilistic model of chronological errors in layer-counted climate proxies:
734 applications to annually banded coral archives, *Clim. Past*, *10*(2), 825–841, doi:10.5194/cp-10-
735 825-2014.

736 Conroy, J. L., D. M. Thompson, K. M. Cobb, D. Noone, S. Rea, and A. N. LeGrande (2017),
737 Spatiotemporal variability in the δ^{18}O-salinity relationship of seawater across the tropical
738 Pacific Ocean, *Paleoceanography*, *32*(5), 484–497, doi:10.1002/2016PA003073.

739 Corrège, T. (2006), Sea surface temperature and salinity reconstruction from coral geochemical
740 tracers, *Palaeogeogr. Palaeoclimatol. Palaeoecol.*, *232*(2-4), 408–428,
741 doi:10.1016/j.palaeo.2005.10.014.

742 Dee, S., J. Emile-Geay, M. N. Evans, A. Allam, E. J. Steig, and D. M. Thompson (2015), PRYSM:
743 An open-source framework for PRoxY System Modeling, with applications to oxygen-isotope
744 systems, *J. Adv. Model. Earth Syst.*, *7*(3), 1220–1247, doi:10.1002/2015MS000447.

745 DeLong, K. L., T. M. Quinn, F. W. Taylor, C.-C. Shen, and K. Lin (2013), Improving coral-base
746 paleoclimate reconstructions by replicating 350 years of coral Sr/Ca variations, *Palaeogeogr.*
747 *Palaeoclimatol. Palaeoecol.*, *373*(C), 6–24, doi:10.1016/j.palaeo.2012.08.019.

748 DeLong, K. L., T. M. Quinn, F. W. Taylor, K. Lin, and C.-C. Shen (2012), Sea surface temperature
749 variability in the southwest tropical Pacific since AD 1649, *Nature Climate Change*, *2*(11),
750 799–804, doi:10.1038/nclimate1583.

751 Deser, C., A. S. Phillips, R. A. Tomas, Y. Okumura, M. A. Alexander, A. Capotondi, J. D. Scott,
752 Y.-O. Kwon, and M. Ohba (2012), ENSO and Pacific decadal variability in the Community
753 Climate System Model version 4, *J. Clim.*, *25*, 2622–2651, doi:10.1175/JCLI-D-11-00301.1.

754 Deser, C., M. A. Alexander, S.-P. Xie, and A. S. Phillips (2010), Sea surface temperature
755 variability: Patterns and mechanisms, *Annu. Rev. Marine. Sci.*, *2*(1), 115–143,
756 doi:10.1146/annurev-marine-120408-151453.

757 DiNezio, P. N., G. A. Vecchi, and A. C. Clement (2013), Detectability of changes in the Walker
758 circulation in response to global warming, *J. Climate*, *26*(12), 4038–4048, doi:10.1175/JCLI-D-
759 12-00531.1.

760 Emile-Geay, J. et al. (2016), Links between tropical Pacific seasonal, interannual and orbital
761 variability during the Holocene, *Nature Geosci.*, *9*(2), 168–173, doi:10.1038/ngeo2608.

762 Emile-Geay, J., K. M. Cobb, M. E. Mann, and A. T. Wittenberg (2013a), Estimating Central
763 Equatorial Pacific SST Variability over the Past Millennium. Part I: Methodology and
764 Validation, *J. Climate*, *26*(7), 2302–2328, doi:10.1175/JCLI-D-11-00510.1.

765 Emile-Geay, J., K. M. Cobb, M. E. Mann, and A. T. Wittenberg (2013b), Estimating Central
766 Equatorial Pacific SST Variability over the Past Millennium. Part II: Reconstructions and
767 Implications, *J. Climate*, *26*(7), 2329–2352, doi:10.1175/JCLI-D-11-00511.1.

768 Epstein, S., R. Buchsbaum, H. A. Lowenstam, and H. C. Urey (1953), Revised carbonate-water
769 isotopic temperature scale, *Geol. Soc. Am. Bull.*, *64*(11), 1315–1326, doi:10.1130/0016-
770 7606(1953)64[1315:RCITS]2.0.CO;2.

771 Evans, M. N., A. Kaplan, M. C. P. and, 2000 (2000), Intercomparison of coral oxygen isotope data
772 and historical sea surface temperature (SST): Potential for coral-based SST field
773 reconstructions, *Paleoceanography*, *15*(5), 551–563, doi:10.1029/2000PA000498.

774 Evans, M. N., S. E. Tolwinski-Ward, D. M. Thompson, and K. J. Anchukaitis (2013), Applications
775 of proxy system modeling in high resolution paleoclimatology, *Quat. Sci. Rev.*, *76*(c), 16–28,
776 doi:10.1016/j.quascirev.2013.05.024.

777 Fairbanks, R. G., M. N. Evans, J. L. Rubenstone, R. A. Mortlock, K. Broad, M. D. Moore, and C.
778 D. Charles (1997), Evaluating climate indices and their geochemical proxies measured in
779 corals, *Coral Reefs*, *16*(1), S93–S100, doi:10.1007/s003380050245.

780 Fritsch, F. N., R. C. S. J. O. N. Analysis, 1980 (1980), Monotone piecewise cubic interpolation,
781 *SIAM*, *17*(2), 238–246, doi:10.1137/0717021.

782 Gagan, M. K., L. K. Ayliffe, D. Hopley, J. A. Cali, G. E. Mortimer, J. Chappell, M. T. McCulloch,
783 and M. J. Head (1998), Temperature and Surface-Ocean Water Balance of the Mid-Holocene
784 Tropical Western Pacific, *Science*, *279*(5353), 1014–1018, doi:10.1126/science.279.5353.1014.

785 Gagan, M. K., L. K. Ayliffe, J. W. Beck, J. E. Cole, E. Druffel, R. B. Dunbar, and D. P. Schrag
786 (2000), New views of tropical paleoclimates from corals, *Quat. Sci. Rev.*, *19*, 45–64,
787 doi:10.1016/S0277-3791(99)00054-2.

788 Gorman, M. K., T. M. Quinn, F. W. Taylor, J. W. Partin, G. Cabioch, J. A. Austin Jr., B. Pelletier,
789 V. Ballu, C. Maes, and S. Saustrup (2012), A coral-based reconstruction of sea surface salinity

at Sabine Bank, Vanuatu from 1842 to 2007 CE, *Paleoceanography*, *27*(3), doi:10.1029/2012PA002302.

Hathorne, E. C. et al. (2013), Interlaboratory study for coral Sr/Ca and other element/Ca ratio measurements, *Geochem. Geophys. Geosyst.*, *14*(9), 3730–3750, doi:10.1002/ggge.20230.

Hereid, K. A., T. M. Quinn, and Y. M. Okumura (2013a), Assessing spatial variability in El Niño-Southern Oscillation event detection skill using coral geochemistry, *Paleoceanography*, *28*(1), 14–23, doi:10.1029/2012PA002352.

Hereid, K. A., T. M. Quinn, F. W. Taylor, C. C. Shen, R. Lawrence Edwards, and H. Cheng (2013b), Coral record of reduced El Nino activity in the early 15th to middle 17th centuries, *Geology*, *41*(1), 51–54, doi:10.1130/G33510.1.

Hurrell, J. W. et al. (2013), The Community Earth System Model: A Framework for Collaborative Research, *Bull. Amer. Meteor. Soc.*, *94*(9), 1339–1360, doi:10.1175/BAMS-D-12-00121.1.

Jimenez, G., J. E. Cole, D. M. Thompson, and A. W. Tudhope (2018), Northern Galápagos Corals Reveal Twentieth Century Warming in the Eastern Tropical Pacific, *Geophys. Res. Lett.*, *45*(4), 1981–1988, doi:10.1002/2017GL075323.

Kilbourne, K. H., T. M. Quinn, F. W. Taylor, T. Delcroix, and Y. Gouriou (2004), El Niño-Southern Oscillation-related salinity variations recorded in the skeletal geochemistry of a *Porites* coral from Espiritu Santo, Vanuatu, *Paleoceanography*, *19*(4), doi:10.1029/2004PA001033.

LeGrande, A. N., and G. A. Schmidt (2006), Global gridded data set of the oxygen isotopic composition in seawater, *Geophys. Res. Lett.*, *33*(12), 15833–5, doi:10.1029/2006GL026011.

Linsley, B. K., A. Kaplan, and Y. Gouriou (2006), Tracking the extent of the South Pacific Convergence Zone since the early 1600s, *Geochem. Geophys. Geosyst.*, *7*, doi:10.1029/2005GC001115.

Lough, J. M. (2010), Climate records from corals, *WIREs Clim Change*, *1*(3), 318–331, doi:10.1002/wcc.39.

Okumura, Y. M., T. Sun, and X. Wu (2017), Asymmetric Modulation of El Niño and La Niña and the Linkage to Tropical Pacific Decadal Variability, *J. Climate*, *30*(12), 4705–4733, doi:10.1175/JCLI-D-16-0680.1.

Otto-Bliesner, B. L., E. C. Brady, J. Fasullo, A. Jahn, L. Landrum, S. Stevenson, N. Rosenbloom, A. Mai, and G. Strand (2016), Climate Variability and Change since 850 CE: An Ensemble Approach with the Community Earth System Model, *Bull. Amer. Meteor. Soc.*, *97*(5), 735–754, doi:10.1175/BAMS-D-14-00233.1.

Parzen, E. (1962), On estimation of a probability density function and mode, *Ann. Math. Stat.*, *33*(3), 1065–1076, doi: 10.1214/aoms/1177704472.

825 Pearson, K. (1920), Notes on the history of correlation, *Biometrika*, *13*(1), 25,
826 doi:10.2307/2331722.

827 Quinn, T. M., and D. E. Sampson (2002), A multiproxy approach to reconstructing sea surface
828 conditions using coral skeleton geochemistry, *Paleoceanography*, *17*(4), 14–1–14–11,
829 doi:10.1029/2000PA000528.

830 Ren, L., B. K. Linsley, G. M. Wellington, D. P. Schrag, and O. Hoegh-guldberg (2003),
831 Deconvolving the δ18O seawater component from subseasonal coral δ18O and Sr/Ca at
832 Rarotonga in the southwestern subtropical Pacific for the period 1726 to 1997, *Geochim.*
833 *Cosmochim. Acta*, *67*(9), 1609–1621, doi:10.1016/S0016-7037(02)00917-1.

834 Ropelewski, C. F., and M. S. Halpert (1987), Global and regional scale precipitation patterns
835 associated with the El Niño/Southern Oscillation, *Mon. Weather Rev.*, *115*, 1606–1626,
836 doi:10.1175/1520-0493(1987)115<1606:GARSPP>2.0.CO;2.

837 Russon, T., A. W. Tudhope, M. C. G. Research, 2015 (2015), Inferring changes in ENSO amplitude
838 from the variance of proxy records, *Geophys. Res. Lett.*, *42*(4), 1197–1204,
839 doi:10.1002/(ISSN)1944-8007.

840 Sayani, H. R., K. M. Cobb, K. DeLong, N. T. Hitt, and E. R. M. Druffel (2019), Intercolony $\delta^{18}O$
841 and Sr/Ca variability among *Porites* spp. corals at Palmyra Atoll: Towards more robust coral-
842 based estimates of climate, *Geochem. Geophys. Geosyst.*, *20*, doi:10.1029/2019GC008420.

843 Schmidt, G. A. et al. (2014), Using palaeo-climate comparisons to constrain future projections in
844 CMIP5, *Clim. Past*, *10*(1), 221–250, doi:10.5194/cp-10-221-2014.

845 Schrag, D. P. (1999), Rapid analysis of high-precision Sr/Ca ratios in corals and other marine
846 carbonates, *Paleoceanography*, *14*(2), 97–102, doi:10.1029/1998PA900025.

847 Shen, C.-C. et al. (2012), High-precision and high-resolution carbonate ^{230}Th dating by MC-ICP-
848 MS with SEM protocols, *Geochim. Cosmochim. Acta*, *99*(C), 71–86,
849 doi:10.1016/j.gca.2012.09.018.

850 Smith, S. V., R. W. Buddemeier, R. C. Redalje, and J. E. Houck (1979), Strontium-calcium
851 thermometry in coral skeletons, *Science*, *204*(4391), 404–407,
852 doi:10.1126/science.204.4391.404.

853 Stevenson, S., B. S. Powell, M. A. Merrifield, K. M. Cobb, J. Nusbaumer, and D. Noone (2015),
854 Characterizing seawater oxygen isotopic variability in a regional ocean modeling framework:
855 Implications for coral proxy records, *Paleoceanography*, *30*, 1573–1593,
856 doi:10.1002/2015PA002824.

857 Stevenson, S., H. V. McGregor, S. J. Phipps, and B. Fox-Kemper (2013), Quantifying errors in
858 coral-based ENSO estimates: Toward improved forward modeling of δ18O, *Paleoceanography*,
859 *28*(4), 633–649, doi:10.1002/palo.20059.

860 Sun, T., and Y. M. Okumura (2019), Role of Stochastic Atmospheric Forcing from the South and
861 North Pacific in Tropical Pacific Decadal Variability, *J. Climate*, *32*(13), 4013–4038,
862 doi:10.1175/JCLI-D-18-0536.1.

863 Thompson, D. M., T. R. Ault, M. N. Evans, J. E. Cole, and J. Emile-Geay (2011), Comparison of
864 observed and simulated tropical climate trends using a forward model of coral $\delta^{18}O$, *Geophys.*
865 *Res. Lett.*, *38*(14), L14706, doi:10.1029/2011GL048224.

866 Thyng, K., C. Greene, R. Hetland, H. Zimmerle, and S. DiMarco (2016), True colors of
867 oceanography: Guidelines for effective and accurate colormap selection, *Oceanog*, *29*(3), 9–13,
868 doi:10.5670/oceanog.2016.66.

869 Trenberth, K. E. (1997), The definition of El Niño, *Bull. Amer. Meteor. Soc.*, *78*(12), 2771–2777,
870 doi:10.1175/1520-0477(1997)078<2771:TDOENO>2.0.CO;2.

871 Trenberth, K. E., and T. J. Hoar (1996), The 1990–1995 El Niño-Southern Oscillation event:
872 Longest on record, *Geophys. Res. Lett.*, *23*(1), 57–60, doi:10.1029/95GL03602.

873 Weber, J. N. (1973), Incorporation of strontium into reef coral skeletal carbonate, *Geochim.*
874 *Cosmochim. Acta*, *37*(9), 2173–2190, doi:10.1016/0016-7037(73)90015-X.

875 Weber, J. N., and P. M. J. Woodhead (1972), Temperature dependence of oxygen-18 concentration
876 in reef coral carbonates, *Journal of Geophysical Research: Oceans*, *77*(3), 463–473,
877 doi:10.1029/JC077i003p00463.

878 Wittenberg, A. T. (2009), Are historical records sufficient to constrain ENSO simulations?
879 *Geophys. Res. Lett.*, *36*(12), 3–5, doi:10.1029/2009GL038710.

880 Wittenberg, A. T., A. Rosati, T. L. Delworth, G. A. Vecchi, and F. Zeng (2014), ENSO Modulation:
881 Is It Decadally Predictable? *J. Climate*, *27*(7), 2667–2681, doi:10.1175/JCLI-D-13-00577.1.

Under review in Paleoceanography and Paleoclimatology (submitted December 16, 2019)

Supporting Information for

Developing a coral proxy system model to compare coral and climate model estimates of changes in paleo-ENSO variability

A.E. Lawman[1,2]*, J.W. Partin[1], S.G. Dee[3], C.A. Casadio[1], P. Di Nezio[1], T.M. Quinn[1,2]

[1]Institute for Geophysics, Jackson School of Geosciences, The University of Texas at Austin, Austin, TX, USA. [2]Department of Geological Sciences, Jackson School of Geosciences, The University of Texas at Austin, Austin, TX, USA. [3]Department of Earth, Environmental and Planetary Sciences, Rice University, Houston, TX, USA.

Contents of this file

Introduction

The supporting information includes two figures that demonstrate the age model algorithm (Section 3.3) for mean-removed pseudocoral $\delta^{18}O$ ($\Delta\delta^{18}O_{pseudocoral}$). Selected sites include Christmas Island in the central equatorial Pacific (2°N, 157°W) and Vanuatu in the southwest Pacific (16°S, 167°E). Coral $\delta^{18}O$ is forward modeled as a linear combination of sea-surface temperature and salinity using the sensor model of *Thompson et al.* [2011] (Section 2.2.1). Surface temperature and salinity data come from the CESM Last Millennium Ensemble 850 control [*Otto-Bliesner et al.*, 2016] (Section 2.1). Refer to the Section 3.3 in the main text for age modeled SST derived from coral Sr/Ca ($SST_{Sr/Ca}$).

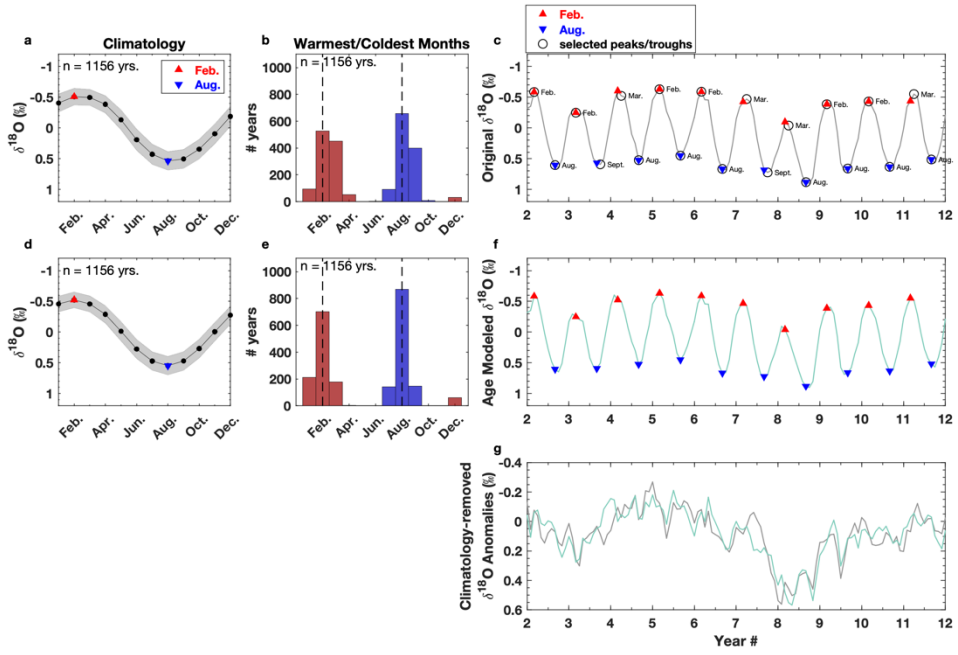

Figure S1. Age modeling $\Delta\delta^{18}O_{pseudocoral}$ at Vanuatu. Same as Figure 4 in the main text except for forward modeled $\Delta\delta^{18}O_{pseudocoral}$ at the model grid point closest to Vanuatu.

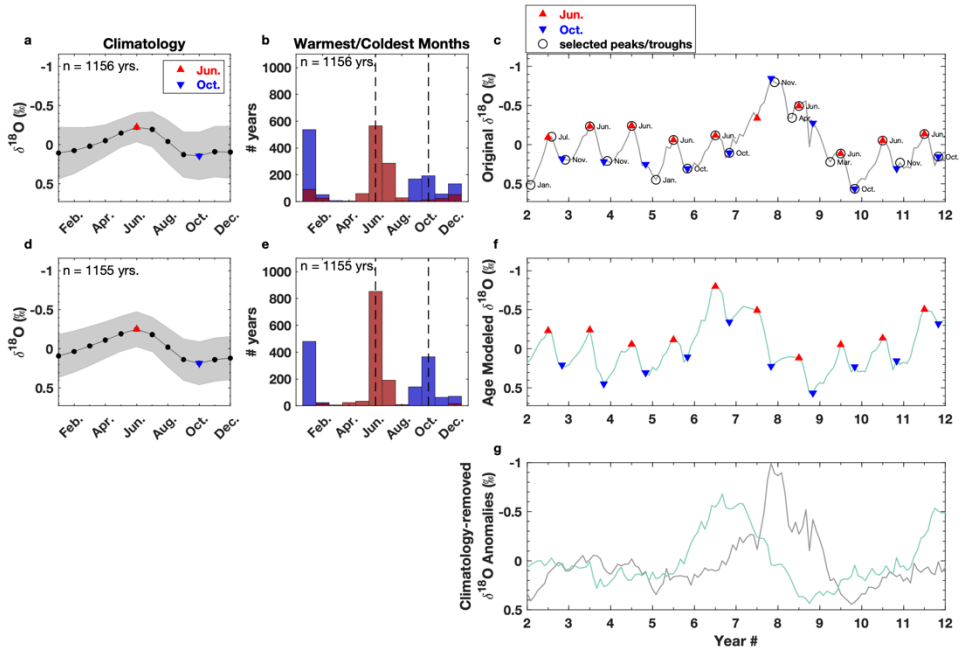

Figure S2. Age modeling $\Delta\delta^{18}O_{pseudocoral}$ at Christmas Island. Same as Figure 4 in the main text except for forward modeled $\Delta\delta^{18}O_{pseudocoral}$ at the model grid point closest to Christmas Island.